crystals

MDPI

Article

D,L-Citrullinato-bipyridine Copper Complex: Experimental and Theoretical Characterization

Diego Ramírez-Contreras [1], Amalia García-García [1,2], Angel Mendoza [1], Laura E. Serrano-de la Rosa [3], Brenda L. Sánchez-Gaytán [1], Francisco J. Melendez [4], María Eugenia Castro [1,*] and Enrique González-Vergara [1,*]

[1] Centro de Química del Instituto de Ciencias, Benemérita Universidad Autónoma de Puebla, 18 Sur y Av. San Claudio, Col. San Manuel, Puebla 72570, Mexico; angel.mendoza@correo.buap.mx (A.M.)
[2] Departamento de Química Inorgánica, Facultad de Ciencias, Universidad de Granada, Av. Fuente Nueva s/n, 18003 Granada, Spain
[3] Laboratorio Central del Instituto de Física "Luis Rivera Terrazas" (IFUAP), Benemérita Universidad Autónoma de Puebla, 18 Sur y Av. San Claudio, Col. San Manuel, Puebla 72570, Mexico
[4] Facultad de Ciencias Químicas, Benemérita Universidad Autónoma de Puebla, 18 Sur y Av. San Claudio, Col. San Manuel, Puebla 72570, Mexico
* Correspondence: mareug.castro@correo.buap.mx (M.E.C.); enrique.gonzalez@correo.buap.mx (E.G.-V.); Tel.: +52-222-363-0623 (E.G.-V.)

Abstract: Citrulline is a non-protein amino acid that acts as a metabolic intermediate in the urea cycle and arginine synthesis. It is present in some foods, although its name derives from watermelon (*Citrullus vulgaris*), from which it was first identified. Under normal conditions, Citrulline exists as a zwitterion in aqueous solutions since its carboxylic and amine groups can act as Lewis donors to chelate metal cations. In addition, Citrulline possesses in the aliphatic chain a terminal ureide group, which could also coordinate. Although Citrulline is comparable to other classical amino acids, its coordination chemistry has yet to be explored. Only two metal complexes have been reported, and the copper complex is a polymeric and insoluble material. As part of our search for active Casiopeina® analogs, we created a more soluble complex by combining 2,2′-Bipyridine into a new mixed material, resulting in the mononuclear complex $[Cu(Bipy)(Citr)(H_2O)(NO_3)]\cdot H_2O$. Single-crystal X-ray diffraction, spectroscopic methods (FT-IR, UV-Vis, Raman), and mass spectrometry characterized the material. Interestingly, both isomers of Citrulline, R(D), and S(L) are present in the same crystal. In addition, the molecular structure and electronic properties of the complex were calculated using density functional theory (DFT). Non-covalent interactions were characterized using the atoms-in-molecules (AIM) approach and Hirshfeld surface (HS) analysis. This ternary complex containing Citrulline and 2,2′-Bipyridine will be used for docking calculations and preliminary biological studies using calf thymus DNA (CT-DNA) and plasmid pUC19 as a first approximation to cytotoxic activity against cancer cell lines.

Keywords: citrulline; 2,2′-Bipyridine; copper complex; DFT; AIM; Hirshfeld surface

Citation: Ramírez-Contreras, D.; García-García, A.; Mendoza, A.; Serrano-de la Rosa, L.E.; Sánchez-Gaytán, B.L.; Melendez, F.J.; Castro, M.E.; González-Vergara, E. D,L-Citrullinato-bipyridine Copper Complex: Experimental and Theoretical Characterization. *Crystals* **2023**, *13*, 1391. https://doi.org/10.3390/cryst13091391

Academic Editor: Vladimir P. Fedin

Received: 31 August 2023
Revised: 15 September 2023
Accepted: 15 September 2023
Published: 19 September 2023

1. Introduction

Citrulline ($C_6H_{13}N_3O_3$) is a non-essential amino acid involved in the body's urea cycle and arginine synthesis [1]. It is a molecule abundant in certain foods, such as watermelon, the fruit from which its name, *Citrullus*, is derived [2]. Wada discovered it in 1914 thanks to synthesizing its complex with copper(II) [3]. This was obtained by reacting watermelon juice with a copper(II) salt, resulting in a deep blue precipitate that was insoluble in neutral to basic solutions [4]. The Citrulline complexes have been well-known for a long time, but they have generated little interest because most researchers have described them as "difficult to crystallize". However, this amino acid has recently garnered considerable interest due to its potential medicinal properties since it improves blood flow and reduces blood pressure; it is used for athletic performance, sickle cell disease, erectile dysfunction,

high blood pressure in the lungs a, and hearth disease [5–8]. Only in the last decade have many papers been published that equal the number of papers since its discovery in 1930 until 2013. Figure 1 presents the schematic representation of the Citrulline molecule.

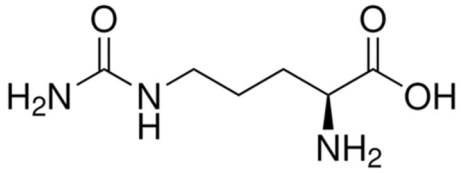

Figure 1. Schematic representation of the Citrulline molecule.

In the physiological environment, Citrulline occurs almost exclusively as a zwitterion. At an alkaline pH, both carboxylic and amine groups can function as Lewis donors so that they can coordinate with metallic cations [9]. However, the non-bonding electrons of the nitrogen atoms are conjugated with double bonds, rendering the lateral chain significantly less capable of forming a complex. Therefore, Citrulline complexes are identical to those formed by conventional amino acids. Even though Kurtz proposed the structure of the copper complex in 1939 [10], it was considered an intermediate in the isolation of Citrulline due to its insolubility; however, spectroscopic approaches employed by Ganadu et al. in 1991 on [Pd(Citr)$_2$] shed light on the structure of the complex [11]. Coordination using the carboxylate and the amino groups was typical of other amino acids, but the function of the ureide moiety was not mentioned. Mascaliovas verified this by identifying the compound as a bis-citrullinate of palladium [12]. Two Citrulline molecules acting as bidentate ligands coordinate the metal in a square planar configuration, with nitrogen and oxygen atoms in *trans*-positions. The crystal belongs to the P-1 space group, necessitating the presence of L- and D-Citrulline since it has an inversion center. Interestingly, the authors omitted this detail. Recently, our research group discovered that the copper complex is a polymeric bidimensional structure and that the ureide group is crucial in coordinating the carbonyl oxygen with the copper [13]. In addition, it was found that, although the synthesis started with L-Citrulline, the polymeric [Cu(Citr)$_2$]$_n$ complex crystallized with D-isomers.

Copper(II) metallodrugs are a promising type of anticancer chemotype because they can generate reactive oxygen species (ROS) and reactive nitrogen species (RNS), which damage and kill cancer cells by causing oxidative damage. Several of these copper complexes can bind or inhibit topoisomerases and DNA. Additionally, these complexes can impair checkpoints of the cell cycle and death effector proteins [14–16]. In this regard, a class of ternary Cu(II) complexes known as "Casiopeinas", with the overall structure [Cu(NN)(OO)]X, exhibit promising in vitro and in vivo anticancer activity. Various Casiopeina complexes with high water solubility have been successful in clinical trials. These complexes are cytotoxic to cisplatin-sensitive or resistant cancer cells [17–19] and are frequently more easily absorbed and utilized by cells.

Our group has investigated Casiopeina-analogs with side chains as auxiliary ligands to increase solubility and hydrogen bond interactions to increase affinity for targeting DNA, RNA, and proteins [20–23]. With this purpose, in this work, we describe the synthesis of a new Citrulline complex with the chemical formula [Cu(Bipy)(Citr)(H_2O)(NO_3)]·H_2O (Compound **1** hereafter). The single-crystal X-ray diffraction technique revealed the coexistence of both D- and L-isomers in the material. The experimental characterization of Compound **1** by spectroscopic techniques (Fourier-transform infrared spectroscopy, UV-visible, and Raman), mass spectrometry, theoretical characterization by using density functional theory (DFT), and the atoms-in-molecules (AIM) approach has been carried out.

2. Materials and Methods

2.1. Materials and Spectroscopic Characterization

Citrulline was purchased from a commercial supplier (Beyond Raw Chemistry Labs, Pittsburgh, PA, USA). The stereoisomer purity was verified by optical rotation, always

using samples with 3.0 or higher angles. All other reagents and solvents were purchased from Sigma-Aldrich® (Merck, Mexico) with ACS purity (98% or higher).

The UV-Vis characterization was performed in a Varian Cary UV-Vis Spectrophotometer using a quartz cuvette with a 1 cm path. The Fourier-transform infrared (FT-IR) spectrum was recorded from 4000 to 400 cm^{-1} using an Attenuated Total Reflectance (ATR) spectrometer, model ALPHA II Platinum, Bruker brand. The Raman spectrum was obtained at room temperature in a backscattering configuration using the 633 nm line of a He-Ne laser as an excitation source using a LabRAM HR-Olympus Micro Raman. Mass spectrometry was performed on a JEOL MStation JMS-700 with the ion source set up for Fast Atomic Bombardment (FAB-MS).

2.2. Synthesis of D,L-[Cu(Bipy)(Citr)(H_2O)(NO_3)]·H_2O (Compound **1**)

Compound **1** was synthesized by a modification of the method of Su et al. for mixed ligand aminoacidatocopper(II) complexes [24]. In 30 mL of methanol, 1 mmol of Citrulline ($C_6H_{13}N_3O_3$) was suspended under constant stirring and heating (≈50 °C). Then, 1 mL of copper nitrate trihydrate ($Cu(NO_3)_2 \cdot 3H_2O$) solution in methanol (1M) was added to the ligand. When all the mixture powder was dissolved, 1 mL of 2,2′-Bipyridine ($C_{10}H_8N_2$) in methanol (1M) was added. The solution remained stirred and heated for 15 min. Subsequently, the product was cooled to room temperature and the pH was increased with potassium hydroxide (KOH) to the 7–8 range. The final solution was left to dry, and the resulting blue powder was redissolved in 3–5 mL of distilled water, filtered with a 0.22 µm syringe filter (Corning), and left to crystallize at room temperature. After 2–3 days, highly water-soluble blue crystalline needles were obtained. Yield ≈ 80%.

2.3. Crystallographic Refinement

A high-quality crystal was subjected to single-crystal X-ray diffraction studies. Data were collected with an Oxford Diffraction Gemini-Atlas diffractometer equipped with a charge-coupled device area detector and graphite monochromated *Mo-Kα* radiation (λ = 0.71073 Å). The CrysAlis PRO and CrysAlis RED software packages were used for data collection and absorption correction [25]. The structure was solved by direct methods using the ShelXT program and refined by full-matrix least-squares on F^2 with SHELXL-2019 [26]. The positional and anisotropic atomic displacement parameters were refined for all non-hydrogen atoms. Hydrogen atoms were located in different Fourier maps and included as fixed contributions riding their parent atoms, with isotropic thermal factors chosen as 1.2 times their carrier atoms. The Olex2 software [27] was used as the graphical interface. Crystallographic data for the structure reported in this paper have been deposited with the Cambridge Crystallographic Data Center (CCDC number 2287583). Crystallographic parameters are presented in Tables 1 and S1–S3.

Table 1. Crystallographic data and structure refinement details of Compound **1**.

[Cu(Bipy)(Citr)(H_2O)(NO_3)]·H_2O	
Chemical formula	$C_{16}H_{24}CuN_6O_8$
M_r ($g \cdot mol^{-1}$)	491.95
Crystal system, space group	Triclinic, P-1
Temperature (K)	293(2)
a, b, c (Å)	7.2136(3), 12.2497(6), 14.1356(6)
α, β, γ (°)	65.430(4), 77.331(3), 82.046(3)
V ($Å^3$)	1106.75(9)
Z	2
Radiation type	Mo *Kα* (λ = 0.71073 Å)
ρ_{cald} ($g \cdot cm^{-3}$)	1.476
μ (mm^{-1})	1.040
Crystal size (mm)	0.32 × 0.25 × 0.20
GoF on F^2	1.054
R_1 [I > 2σ(I)]/[all data]	0.0484/0.0624
wR_2 [I > 2σ(I)]/[all data]	0.1211/0.1295

The crystal structure of Compound **1** contained solvent-containing voids. These solvent molecules could not be refined satisfactorily; thus, the solvent was omitted from the final refinement cycle. The contribution of the missing solvent to the calculated structure factors was considered using the SOLVENT MASK routine of Olex2 [27]. The solvent mask was calculated, and 22 electrons were found in a volume of 88 $Å^3$ in 1 void per unit cell.

2.4. Theoretical Calculations

The molecular structure and the electronic properties of Compound **1** were calculated using density functional theory (DFT) [28] and time-dependent DFT (TD-DFT) [29]. The functional PBEPBE [30] was used with the LANL2DZ [31] basis set. The solvent effect was implicitly included with the universal solvation model using water as a solvent based on solute electron density (SMD) [32]. Calculations were performed without symmetry imposition, and the vibrational frequencies were determined to establish minimum structures on the potential energy surface. UV-Vis, IR, and Raman spectra were calculated. The molecular electrostatic potential (MEP) maps were analyzed. The TD-PBEPBE time-dependent density functional was used for the UV-Vis spectrum calculation, with the same basis set in the vertical absorption approach [33]. The calculations were performed with the Gaussian 16 program [34], and the visualization of the results was performed with the GaussView 6.0.16 program [35]. Also, the main non-covalent interactions of Compound **1** were studied using the atoms-in-molecules (AIM) approach and AIMAll software [36]. The Hirshfeld surface and 2D fingerprint analyses were conducted using X-ray structures and CrystalExplorer 17.5 software [37].

3. Results

3.1. Structural Description of Compound **1**

Single-crystal X-ray diffraction analysis revealed that Compound **1** crystallizes in the triclinic P-1 space group. The unit cell consists of mononuclear entities of [Cu(Bipy)(Citr)$(H_2O)(NO_3)$] with water molecules of crystallization around them. The metal center established a CuO_3N_3 sphere with a distorted octahedral geometry with elongated deformation (Figures 2 and S1). One oxygen atom from the coordinated water molecule and one oxygen atom from the nitrate anion are each present in the apical positions. In the equatorial plane, one oxygen and one nitrogen atom pertain to the carboxyl and amino groups of the Citrulline ligand, and two nitrogen atoms are part of the 2,2′-Bipyridine ligand. The elongated deformation in the coordination sphere is attributed to the high Jahn–Teller effect that undergoes Cu(II) in octahedral geometry; the d orbitals tend to split to remove the degenerate energy levels and thus lower the system's energy [38]. For that reason, whereas basal positions are occupied by three Cu-N and one Cu-O bond with distances in the range of 1.983(2)–2.010(2) Å and 1.9287(17) Å, respectively, the apical positions are defined by Cu-O_{water} of 2.485 Å and Cu-$O_{nitrate}$ of 2.763 Å, corresponding to electrostatic interactions [39].

Due to the presence of a chiral carbon (C8 atom) in the Citrulline ligand, the mononuclear entity exhibits two enantiomers. As shown in Figure 3, both enantiomers are present in the unit cell. Although not only the D–L configurations are present in each cell, we only see the average across the packing. Therefore, the presence of the enantiomers with the same absolute configuration in the cell cannot be observed, and in this case, the probability is 50–50 for each one. In Figure S2, the three possibilities are presented.

Finally, the mononuclear compounds interact through intermolecular hydrogen bonds between the coordinated water molecule and the carboxylate group of another compound. In addition, each compound interacts with a third entity thanks to the water molecule of crystallization, which joins the carboxyl group of one entity and the ureide group of another (Figure 4 and Table 2).

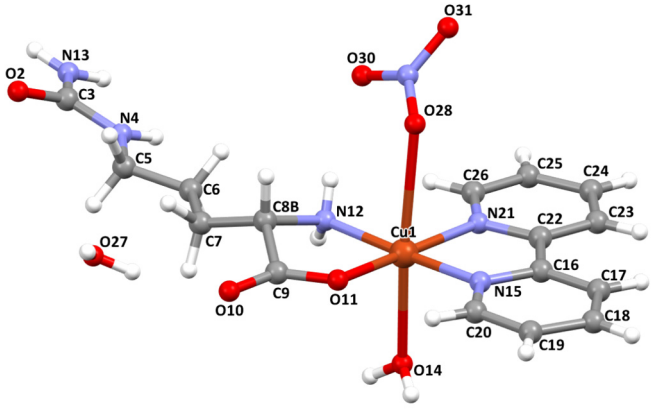

Figure 2. The mononuclear entity of Compound **1**, with general formula S(L)-[Cu(Bipy)(Citr)(H_2O)(NO_3)]·H_2O.

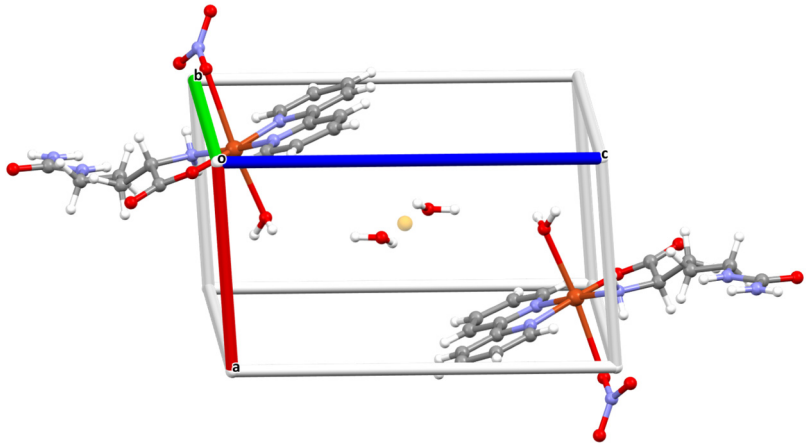

Figure 3. The unit cell of Compound **1**. The orange point in the center corresponds to the centroid of the structure, as well as its inversion center.

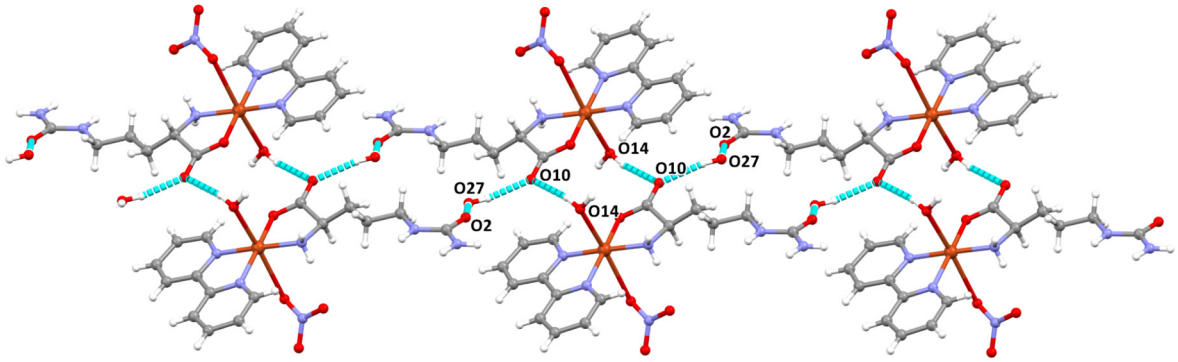

Figure 4. Each entity is joined to another by two hydrogen bonds between the coordinated water molecules (O14) and the carboxyl groups (O10) of Citrulline and to a third monomer thanks to the crystallization water molecule (O27) and the ureide group (O2).

Table 2. Lengths (Å) and angles (°) for selected hydrogen bonds in Compound **1**.

D-H···A	Distance D-H	Distance H···A	Distance D···A	Angle
O14-H14B···O10 [i]	0.85	1.95	2.788(3)	168.3
O27-H27A···O2 [ii]	0.85	1.96	2.806(3)	172.3
O27-H27B···O10	0.85	1.99	2.825(3)	168.2

Symmetry operations: i = 1-x, 1-y, 2-z; ii = 1-x, 2-y, 1-z.

3.2. UV-Visible Spectroscopy

UV-visible spectra of copper complexes with amino acids exhibit a $d \rightarrow d$ transition as unsymmetrical broadband with a maximal intensity of 700–550 nm, with a maximum at 610 nm, and a molar absorptivity $\varepsilon = 6.06 \times 10^1\ M^{-1}\ cm^{-1}$. (Figure 5). As shown in Figure 5, a tetragonally deformed octahedral environment is suggested for the copper(II) ion. The $d \rightarrow d$ band comprises three electronic dipole transitions that overlap and are associated with the three spin-allowed states, transitions, $2A_{1g}(dz^2) \rightarrow 2B_{1g}(dx^2–y^2)$, $2E_g(dyz \approx dxz) \rightarrow 2B_{1g}(dx^2–y^2)$, and $2B_{2g}(dxy) \rightarrow \approx 2B_{1g}(dx^2–y^2)$, respectively [40,41].

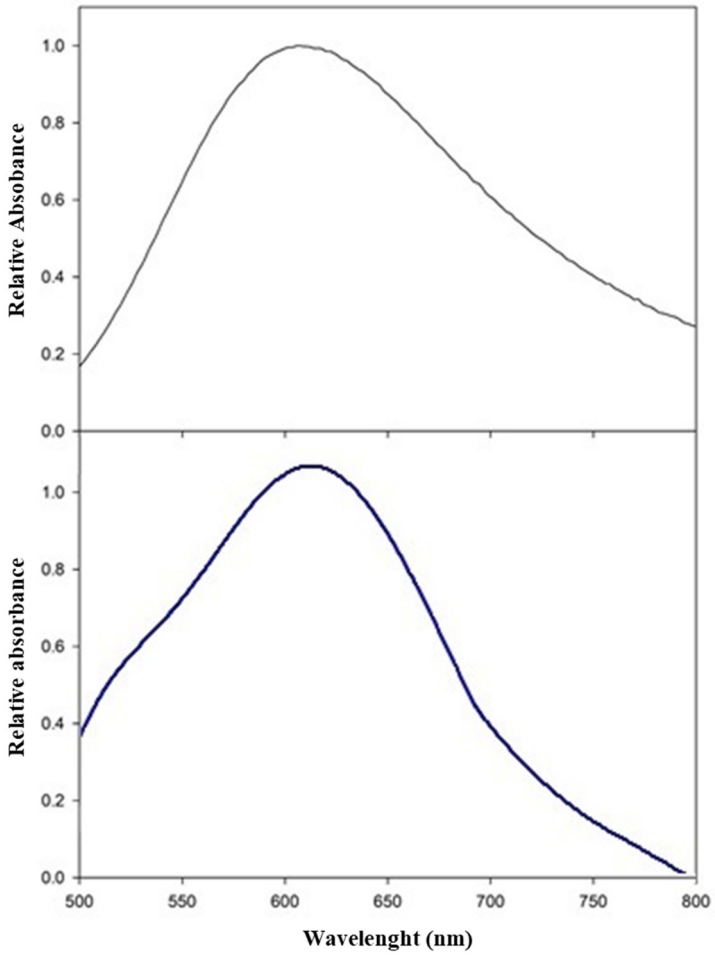

Figure 5. Electronic spectrum of $[Cu(Bipy)(Citr)(H_2O)(NO_3)]$ in the 500–800 nm range, ca. = 15 mg/mL. (black line) and calculated spectrum at the level of theory PBEPBE/LANL2DZ (blue line).

Experimental and theoretical electronic spectra were compared and measured from 500 to 800 nm (Figure 5). The calculated absorption wavelengths (λ_{theo}), excitation energies ($E_{exc.}$), oscillator strengths (f), and assignment of the electronic transitions are presented in Table 3.

TD-PBEPBE functional confirms that the strong transition is at 617 nm with an excitation energy of 2.01 eV and oscillator strength f = 0.0049, which is assigned to $d \rightarrow d$ transitions. In general, Table 3 shows good agreement between TD-DFT calculations and the experimental measurements at the 700–550 nm range; the whole transition belongs to the visible region. The maximum experimental absorption band is observed at 610 nm with the fundamental contribution of the HOMO and LUMO orbitals. However, the broadest band is assigned to $d \rightarrow d$ transitions with low intensity but a relatively high contribution of the frontier molecular orbitals. The TD-PBEPBE functional predicted reliable results for the

electronic transitions and excitation energies of compound [Cu(Bipy)(Citr)(H_2O)(NO_3)] (see Figure 5 and Table 3).

Table 3. Experimental absorption wavelengths (λ_{exp}), calculated absorption wavelengths (λ_{theo}), excitation energies ($E_{exc.}$), oscillator strengths (f), and significant contributions of the electronic transitions of [Cu(Bipy)(Citr)(H_2O)(NO_3)] calculated at PBEPBE/LANL2DZ level of theory.

λ_{exp} (nm)	λ_{theo} (nm)	$E_{exc.}$ (eV)	Osc. Strengths	Major Contributions
700	786	1.58	0.0010	H-1→L + 1 (3%)
	656	1.89	0.0001	H-3→L (5%)
610	617	2.01	0.0049	H→L (97%)
	608	2.04	0.0002	H-5→L (60%)
	602	2.06	0.0001	H-1→L (44%)
550	544	2.28	0.0003	H-8→L + 1 (5%)
	513	2.42	0.0002	H-7→L + 2 (1%)
	506	2.45	0.0001	H-4→L + 5 (2%)

In Figure 6, the UV spectrum corresponds to π-π* intraligand of the Bipyridine (300 nm) and a MLCT with stolen intensity (312 nm) ($\varepsilon(300) = 1.43 \times 10^4$ M^{-1} cm^{-1}; $\varepsilon(312) = 1.35 \times 10^4$ M^{-1} cm^{-1}) [42].

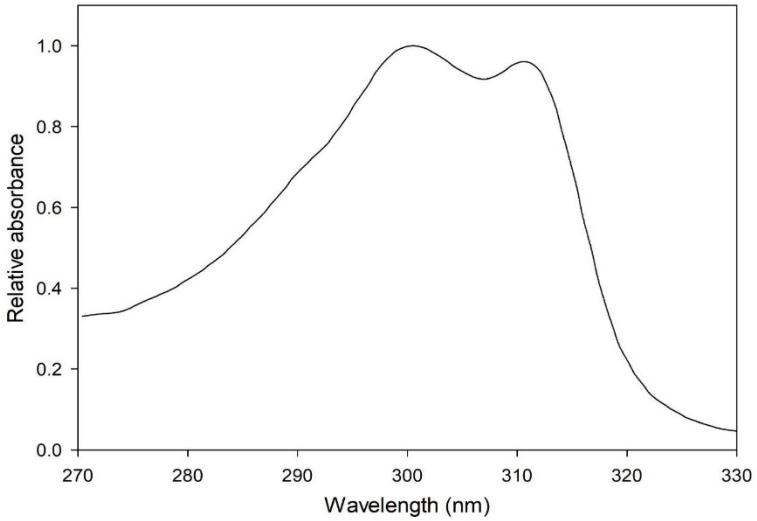

Figure 6. Electronic spectrum of [Cu(Bipy)(Citr)(H_2O)(NO_3)] in the 270–330 nm range, ca. = 0.01 mg/mL.

3.3. Infrared Spectroscopy

Figure 7 depicts the Infrared spectrum of the synthesized complex. Three important regions of the spectrum are worth mentioning. The first refers to peaks in the 3500–2800 cm^{-1} region, which are predominantly attributable to coordinated H_2O molecules and amide (NH_2) asymmetric and symmetric absorption bands, followed by stretching vibrations of amide (NH) of the Citrulline and aromatic (CH) stretching of the Bipyridine which are close but above 3000 cm^{-1}. Two adjacent faint peaks in the 2960–2860 cm^{-1} region belong to the (CH) asymmetric and symmetric vibrations of the aliphatic chain of the Citrulline. The set of assignments between 1700 and 1350 cm^{-1} corresponds to the stretching vibrations of the carbonyl group, and the asymmetric stretching of the carboxyl group gives strong broadband at 1605 cm^{-1}. The intense band at 1538 cm^{-1} and the small band at 1475 cm^{-1} correspond to the scissoring modes of (NH_2) amino and amide groups. The peak at 1396 cm^{-1} can be assigned to symmetric carboxylate stretching. At 1326 cm^{-1} and 1310 cm^{-1}, there are intense split bands of nitrate ion $\nu_{as}(NO_3)$ and less intense bands of $\nu_s(NO_3)$ at 1034 cm^{-1}, indicating the presence of monodentate coordinating NO_3^- ion.

Finally, in the region below 1000 cm^{-1}, the characteristic peak of Bipyridine at 775 cm^{-1} corresponds to the out-of-plane bending mode [43,44].

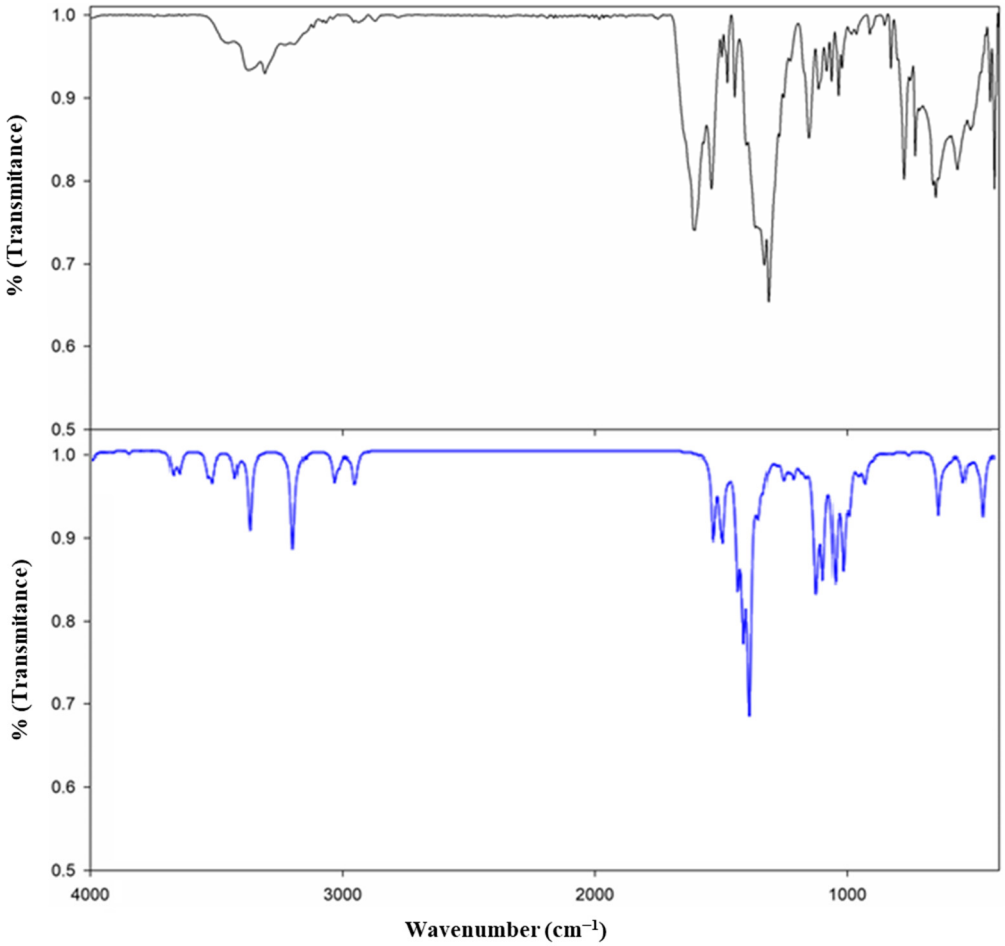

Figure 7. FTIR spectra of Compound 1: Experimental (black line) and calculated (blue line).

A vibrational analysis based on a comparison of the calculated and experimental normal vibration modes was carried out to confirm the binding mode of the complex. The vibrational spectrum of [Cu(Bipy)(Citr)(H_2O)(NO_3)] complex with a 0.950 scale factor is discussed, and the results are presented in Table 4. According to the results obtained at the PBEPBE/LANL2DZ level of theory, the two first bands calculated at 3495 and 3472 cm^{-1} are due to the $\nu_{as}(OH)_w$ and $\nu_{as}(NH_2)_{amide}$ vibrational mode of water (65%) and amide (76%), respectively. Additionally, the broadband at the range of 3367 to 3269 cm^{-1} is assigned to the combination of the symmetric (64%) and asymmetric (11%) modes of the amine group, as well as the asymmetric (87%) mode of the amino group. The PED values of the bands between 3029 and 3013 cm^{-1} confirm the presence of the asymmetric modes of stretching for the pyridine ring and aliphatic chain of the Citrulline. The band observed at 1605 cm^{-1} agrees with the calculated at 1543 cm^{-1}, which corresponds to C=O length changes and HOH bending of water in the complex. On the other hand, the band observed in the IR spectrum at 1538 and 1475 cm^{-1} are associated, according to calculations, with the HNH in-plane bending or scissoring of the amino and amide groups in the Citrulline. The result calculated to the band at 1410 cm^{-1} assigned in the IR spectrum at 1396 cm^{-1} confirms the presence of $\nu_{as}(O=C)_{carboxylate\ group}$ symmetric normal mode (63%) through the C=O length change and the $\delta(NH_2)_{amino}$ bending normal mode (68%). These values support the possible bidentate binding of the Citruline molecule through the $O_{carboxylic}$ and the N_{amino} atoms.

Table 4. FTIR experimental vibrational frequencies of [Cu(Bipy)(Citr)(H_2O)(NO_3)] and FTIR calculated vibrational frequencies (scaled with 0.950 factor) at the PBEPBE/LANL2DZ level of theory.

Experimental (cm^{-1})	PBEPBE (cm^{-1})	Assignments PED (%)
3461	3495	65 $\nu_{as}(OH)_w$
3451	3472	76 $\nu_{as}(NH_2)_{amide}$
	3367	
3375−3216	3351	64 $\nu_s(NH_2)_{amide}$ + 11 $\nu_{as}(NH)_{amide}$
	3269	87 $\nu_{as}(NH_2)_{amino}$
3066−3000	3029	28 $\nu_s(CH)_{ring1\_py}$ + 55 $\nu_{as}(CH)_{ring2\_py}$
	3013	63 $\nu_{as}(CH)_{ring1\_py}$ + 31 $\nu_{as}(CH)_{ring2\_py}$
2960−2860	2874	5 $\nu_s(CH)_{aliph}$ + 23 $\nu_{as}(CH)_{aliph}$ + 21 $\nu_{as}(CH)_{aliph}$ + 25 $\nu_{as}(CH)_{aliph}$
	2832	11 $\nu_s(CH)_{aliph}$ + 15 $\nu_s(CH)_{aliph}$ + 24 $\nu_{as}(CH)_{aliph}$ + 26 $\nu_{as}(CH)_{aliph}$
1605	1543	72 $\nu(C=O)_{carboxyl\ group}$ + 9 $\delta(HOH)_w$
1538	1520	68 $\delta(NH_2)_{amino}$
1475	1509	87 $\delta(NH_2)_{amide}$
1396	1410	63 $\nu_{as}(O=C)_{carboxylate\ group}$ + 27 $\delta(O=C–O^-)_{carboxylate\ group}$
1326	1341	85 $\nu_{as}(NO_3)_{free}$
775	809	95 $\tau(CH)_{bipy}$
	471	56 $\nu(Cu=O)_{carbonyl\ group}$
	266	49 $\nu(Cu–O_w)$
	232	53 $\nu(Cu–O_{NO3})$

According to PBEPBE calculations, the following IR bands observed in our [Cu(Bipy)(Citr)(H_2O)(NO_3)] complex were assigned to the $\nu_{as}(NO_3)_{free}$ mode (85%) and $\tau(CH)_{bipy}$ mode (95%) with vibrational frequencies at 1341 cm^{-1} and 809 cm^{-1}, respectively, which are in good agreement with the bands observed and with the literature data reported. Finally, based on DFT calculations, it is possible to predict the bands that appear in the region of 471, 266, and 232 cm^{-1} and that correspond to the $\nu(Cu=O)_{carbonyl\ group}$,$\nu(Cu–O_w)$ and $\nu(Cu–O_{NO3})$ vibrational modes, respectively.

3.4. Raman Spectroscopy

The experimental and theoretical Raman vibrational frequencies of Compound **1** are collected in Table 5. In the same way as the IR analysis, the theoretical Raman spectrum agrees with the experimental values obtained in this work (Figure 8). The typical bands of Bipyridine complexes are 3077 cm^{-1} for the rings C-H and 766 cm^{-1}, corresponding to the C-H out-of-plane bending mode [45]. Most of the other bands overlap with the bands of Citrulline and are difficult to assign. The bands of Citrulline coincide with values previously reported by Baran et al. for Cu(II) complexes with different amino acids [46]. The stretching mode of the hydrogen linked to C (CH) is theoretically assigned at about 2955 cm^{-1}. The pure symmetric modes of the hydrocarbon chain's sym(CH_2) and sym(CH) modes are represented by the small Raman vibrational bands seen in Figure 8 in the 3000–2850 cm^{-1} range. A coupled mode corresponding to the scissoring mode(CH_2) of the hydrocarbon chain coupled with the stretching mode of the carboxylic group (O=C–O^-) and ring stretching (C=C, C=N) could be assigned to the intense band at 1318 cm^{-1}. The nitrate ion could be recognized with a strong peak at 1036 cm^{-1} [47–49].

Table 5. FT-Raman experimental vibrational frequencies of [Cu(Bipy)(Citr)(H_2O)(NO_3)] and FT-Raman calculated frequencies (scaled with 0.950 factor) at the PBEPBE/LANL2DZ level of theory.

Experimental (cm^{-1})	PBEPBE (cm^{-1})	Assignments PED (%)
	3217	86 $\nu_s(OH)_w$
3166	3159	89 $\nu_s(NH_2)_{amino}$
3077	3042	46 $\nu_s(CH)_{ring1\_py}$ + 46 $\nu_s(CH)_{ring2\_py}$
2955	2928	9 $\nu_s(CH)_{aliph}$ + 31 $\nu_s(CH)_{aliph}$ + 29 $\nu_s(CH)_{aliph}$ + 15 $\nu_s(CH)_{aliph}$
2850	2859	45 $\nu_s(CH)_{aliph}$ + 13 $\nu_s(CH)_{aliph}$
1318	1312	89 $\nu_s(NO_3)_{free}$
1036	1045	14 $\nu_s(O=C–O^-)_{carboxylate\ group}$ + 65 $\nu_s(NH_2)_{amino}$ + 10 $\nu_s(NO_3)_{ion}$
766	764	89 $\omega(CH)_{bipy}$

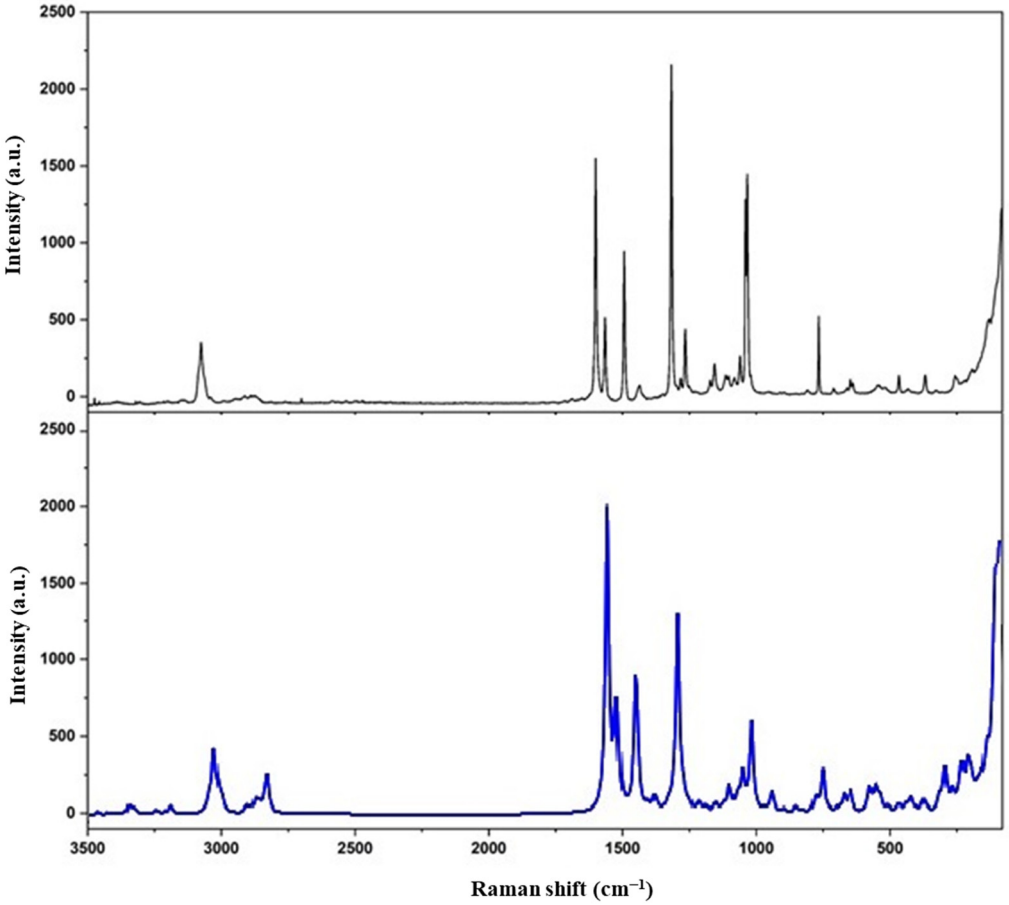

Figure 8. Raman Spectrum of Compound **1**. Experimental (black line), Calculated (blue line).

3.5. Mass Spectrometry

The mass spectrum shows several peaks, as shown in Figure 9. The most important assignments can be made in three groups. The first group corresponds to the 456 and 393 peaks that are close to the molecular weight of $[Cu(C_6H_{12}N_3O_3)(C_{10}H_8N_2)(NO_3)]$ and $[Cu(C_6H_{12}N_3O_3)(C_{10}H_8N_2)]^+$ species, the neutral and ion complex, respectively, which supports the complex formation. The second group can be assigned to decomposition products of the complex; the 375, 219, and 154 peaks are closer to $[Cu(Bipy)_2]^{+2}$, $[Cu(Bipy)]^{+2}$, and (Bipy) molecular weights, respectively. The third assignment corresponds to molecular debris resulting from the degradation of ligands in the molecule, with the 136 and 89 peaks being possible degradation products of Citrulline and Bipyridine. The small peak at 518 could correspond to a small impurity of the dinitrate complex.

3.6. Molecular Structure and Non-Covalent Interactions

Figure 10a shows the optimized structure and Figure 10b shows the molecular electrostatic potential (MEP) of Compound **1** (only the L-isomer will be presented from now on). In Figure 10a, it is observed the L-complex where Cu1 is coordinated with Citrulline and 2,2′-Bipyridine in equatorial sites with distances of Cu1–O1 2.020 Å and Cu1–N1 2.031 Å, and Cu1–N2 and Cu1–N3 2.012–2.038 Å, respectively. The axial positions are occupied by NO_3^- ion and H_2O molecules. The NO_3^- ion is coordinated with Cu1 with a distance of Cu1–O3 3.010 Å, while H_2O is coordinated with Cu1 with a distance of Cu1–O6 3.030 Å. A distorted octahedral geometry around Cu1 is observed. In Figure 10b, the molecular electrostatic potential (MEP) was mapped on the total electronic density with isovalue = 0.0004 a.u. in a range of -1.24×10^{-2} (red zones) to 1.24×10^{-2} (blue zones) of electronic density. The nucleophilic zones (negative charge density) are located on the carboxylate and ureide groups of Citrulline, the NO_3^- ion, and the region occupied by

H_2O. In contrast, the electrophilic zones (deficient density charge) are on the ureide and 2,2′-Bipyridine protons. In addition, yellow and green regions correspond to intermediate electron density zones.

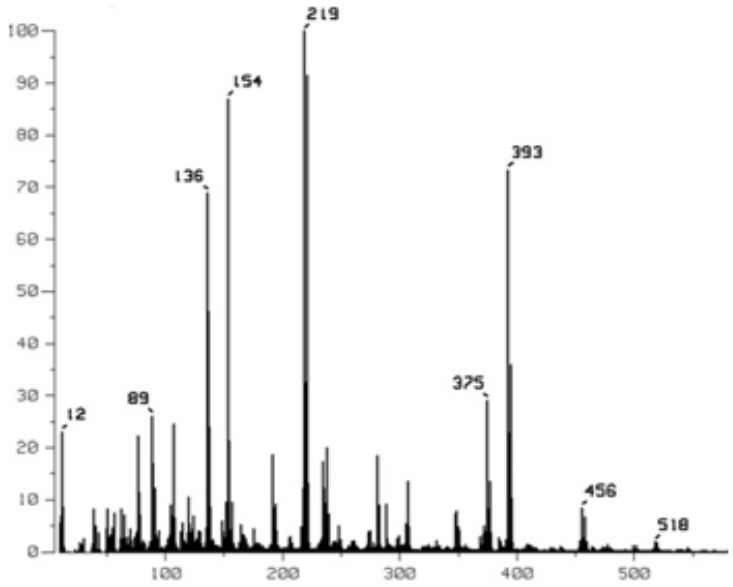

Figure 9. Mass spectrum of Compound **1**.

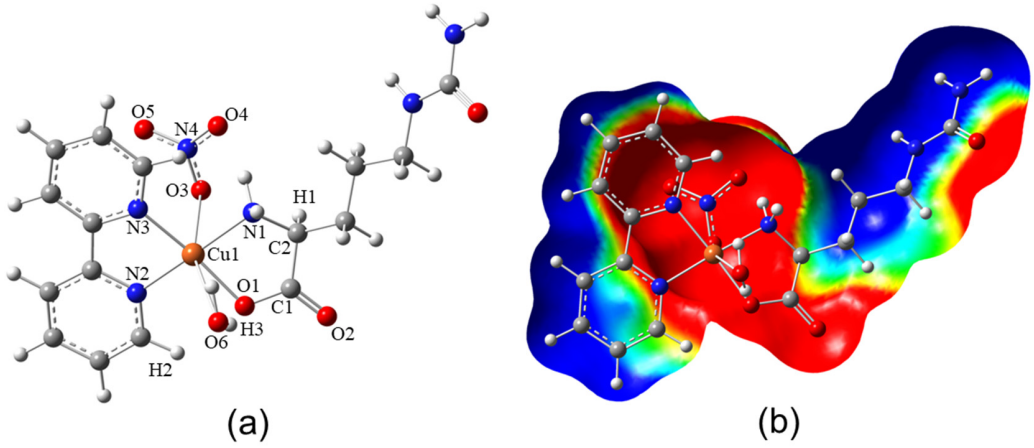

Figure 10. (**a**) Molecular structure of Compound **1** with L configuration; (**b**) Molecular electrostatic potential of Compound **1** with L configuration calculated at the level of theory PBEPBE/LANL2DZ.

The hydrogen bonds were analyzed by electron density, ρ(r), the Laplacian of density, $\nabla^2\rho(r)$, and the interaction energy, $E_{H\cdots Y}$. The results are summarized in Table 6. Figure 11 shows the molecular graphs of Compound **1**. In this figure, green dots represent bond critical points (BCPs) and purple dots represent ring critical points (RCPs). From the results, it can be seen that the ρ(r) on the BCPs is in the range 0.069–0.080 a.u. for Cu1···N1 of the amine group and Cu1···O1 of the carboxylate group of Citrulline, and Cu1···N2 and Cu1···N3 of Bipyridine. The calculated interaction energy ($E_{H\cdots Y}$) is 33.95–40.73 kcal mol^{-1} for these interactions. These values show the significant non-covalent metal-ligand interactions in the equatorial positions coordinated by the Cu1 atom. For the bis-citrullinato Cu(II) complex, values of $E_{H\cdots Y}$ of 40.47 and 44.43 kcal mol^{-1} for Cu1···N1 and Cu1···O1 of Citrulline, respectively, were recently found [13]. Both are comparable with 36.90 and 34.40 kcal mol^{-1} of Compound **1**. Also, similar interaction energies were found for the interactions Cu···N and Cu···O of phenanthroline and glutamine groups at the range of 31.31–50.29 kcal mol^{-1} [22], and of imidazole-pyridine and glycine groups at the range of

37.87–42.20 kcal mol^{-1} [20]; the Cu···N of metformin and Bipyridine groups at the range of 35.61–47.31 kcal mol^{-1} [50]. Concerning the axial positions, the interaction between Cu1 and the O3 of the NO_3^- ion, Cu1···O3, has an interaction energy of 2.26–2.42 kcal mol^{-1}. On the other hand, Compound **1** does not show the interaction between Cu1 and O6 of the H_2O molecule due to a distorted octahedral geometry, see Figure 10. In bis-citrullinato Cu(II) complex were found interactions Cu···O in axial positions with small values of 1.98 kcal mol^{-1} [13]. Finally, RCPs with ρ(r) of 0.0240 a.u. are observed forming stable ring structures of five atoms around Cu(II) coordinated in both isomers of Compound **1**.

Table 6. Topological parameters (in a.u.) and interaction energies $E_{H\cdots Y}$ ((in kcal mol^{-1}) of Compound **1**, L-isomer. Atom labels correspond to those shown in Figure 11.

BCP	ρ(r)	$\nabla^2\rho(r)$	$E_{H\cdots Y}$
Cu1···O1	0.0687	0.4405	33.95
Cu1···N1	0.0797	0.4018	36.87
Cu1···N2	0.0809	0.4560	40.73
Cu1···N3	0.0756	0.4215	36.36
Cu1···O3	0.0097	0.0230	2.26
H2···O1	0.0090	0.0429	1.79
H3···O1	0.0308	0.1089	8.57

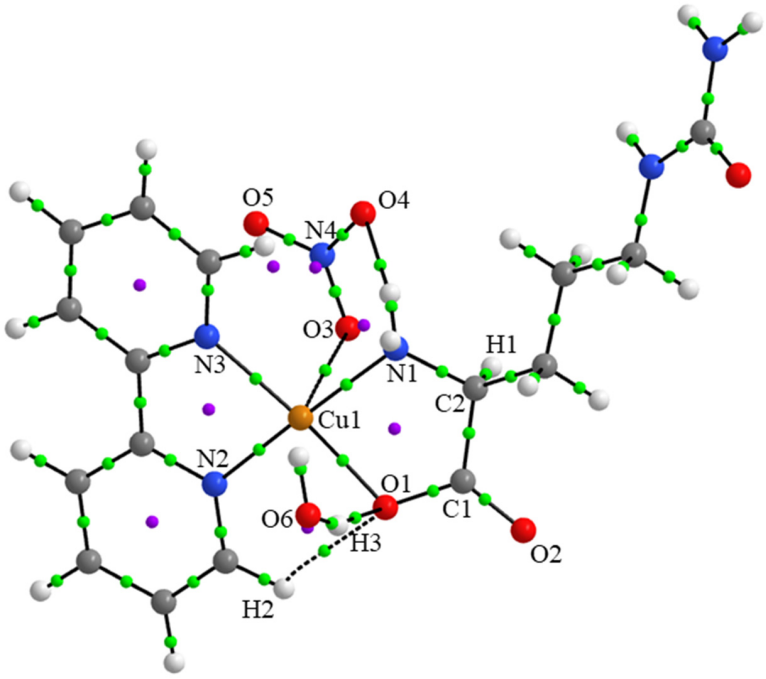

Figure 11. The molecular graph of Compound **1** (L-isomer) shows the main BCPs and RCPs.

Figure 12a shows the Hirshfeld surface (HS) and Figure 12b shows the 2D-fingerprint plot of L-isomer of Compound **1** generated with the function d_{norm}. In Figure 12a, the red spots, labeled as HS1, are due to the hydrogen bonds O–H···O between O6-H3 of water molecule inside HS, acting as a donor, with O2 of carboxylate group outside the HS, acting as acceptor. This interaction contributes 17.1% in HS, as shown in Figure 12b. On the contrary, HS2 corresponds to the carboxylate group inside the HS with adjacent water molecules outside the HS. HS3 is due to the hydrogen bonds between one O atom of NO_3^- ion inside the HS and the H atom of NH_2 groups of the Citrulline molecules outside the HS. In both cases, HS2 and HS3, the O atoms inside of HS act as an acceptor with a contribution of 19.4%, see Figure 11b. The significant contribution to the HS is due to the close intermolecular interactions H···H with 43.0% due to H of Bipyridine with adjacent –NH groups of Citrulline molecules. Other interactions with minor contributions are C···H

(6.1%), H···C (4.1%), C···O (2.0%), O···C (1.6%), and C···C (1.6%). Similar contributions for hydrogen bonds N–H···O connecting Citrulline molecules in bis-citrullinato Cu(II) complex of 17.9% and 21.6% were calculated [13].

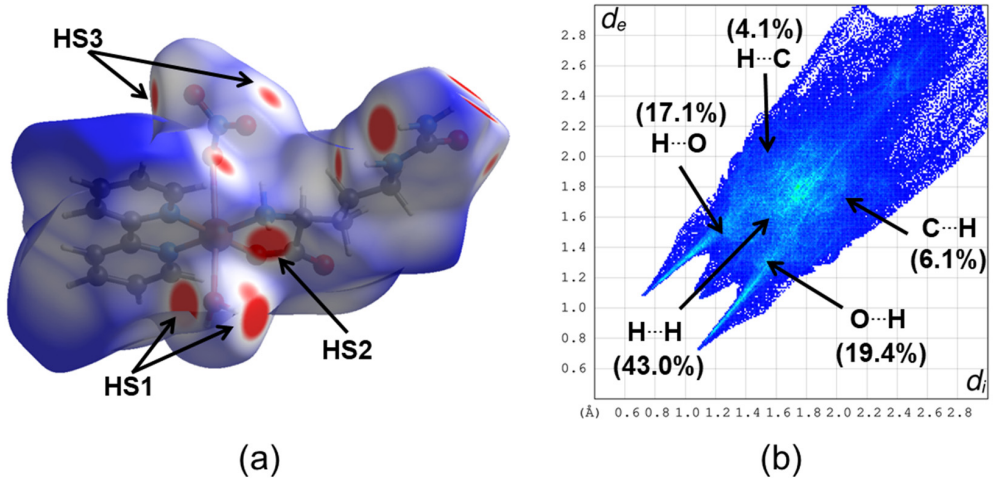

Figure 12. (**a**) Hirshfeld surfaces mapped with the d_{norm} parameter, and (**b**) 2D-fingerprint plot of non-covalent interactions of Compound **1** (L-isomer).

4. Discussion

Citrulline is a very adaptable chemical, potentially generating several hydrogen-bonding contacts since seven strong interactions were observed in its crystal structure [51]. In the case of $[Cu(Citr)_2]_n$, contrary to the case of palladium (II), the oxygen atom of the ureide moiety of the Citrulline occupies the axial positions, generating a highly insoluble polymer. It is important to point out that the configuration of the Citrulline molecule corresponds to the (R) D enantiomer. This could be because of a process called solubility-induced stereoisomer transformation (SIST) [52,53], which leads to racemization and the precipitation of the complex in an inverted form. The theoretical calculations confirmed the distorted octahedral geometry around the Cu(II) ion. The distances of Citrulline and 2,2′-Bipyridine around Cu(II) ion in the equatorial positions are typical non-covalent metal-ligand interactions with high interaction energies analyzed with atom in molecules (AIM) approach. The axial positions occupied by the NO_3^- ion and the H_2O molecule are coordinated with Cu(II) with electrostatic interactions with small values of interaction energies. The Hirshfeld surfaces analysis showed that the most relevant non-covalent interactions are due to hydrogen bonds between water molecules with carboxylate groups of Citrulline of adjacent molecules. Wang et al. [54] have recently proposed a biosorbent based on watermelon grind, and the interaction of Citrulline with Pb(II) throughout its carboxylic acid was claimed based on quantum chemistry simulation. Singh et al. [55] have reported the formation in solution of metal complexes of L-Citrulline/L-tryptophan and thymine with bivalent metal ions, viz. Cu(II), Zn(II), Co(II), and Ni(II), which have been investigated potentiometrically in biologically relevant conditions. The interaction of Citrulline with many metals has been studied in solution [9], but no characterization of the solid state has been performed. Although Citrulline is increasingly recognized as an important nutrient and supplement, only a few examples of its coordination chemistry have been published. Of the only two complexes in the Cambridge database, only one was obtained by single crystal X-ray diffraction and belongs to our research group. In contrast with our previous work (copper bis-citrullinato), a new non-polymeric, water-soluble complex was presented here, which could be considered a Casiopeina-analog.

Casiopeinas are copper(II) coordination compounds, often regarded as the most prominent metal-based drugs with significant anticancer properties [56–58]. These compounds have demonstrated biological efficacy against many types of tumor cells. Both in vitro and in vivo studies have been conducted [18,59], and it is worth noting that Casiopeina III-ia

is now in Phase I of clinical trials. Several mechanisms of action have been hypothesized, encompassing the phenomena of excessive generation of reactive oxygen species (ROS) [60] via the Fenton reaction [61], mitochondrial toxicity [19,62], and direct interaction with DNA. These chemicals can impede cell proliferation and induce cell death by apoptosis [63–65]. Even though these compounds are important because they fight cancer, parasites, and bacteria, new research has been carried out to explore their inhibitory effect against the main protease, Mpro [66]. Mpro is responsible for the replication and primary transcription of the SARS-CoV-2 virus's genetic material. It was concluded that the most studied Casiopeinas could inhibit Mpro more efficiently than free monochelates, bioactive ligands, and boceprevir (a recognized inhibitor). In a recent study by Vázquez-Rodrigez et al. [23], employing density functional theory (DFT) methodology, the optimized molecular structures of seven copper-mixed complexes with amino acids and Bypiridine were obtained. Arginine (Arg), Ornithine (Orn), Lysine (Lys), Citrulline (Citr), Asparagine (Asn), Threonine (The), and Glutamine (Gln) were analyzed by three docking methodologies for their interaction with the active site of TPMRSS2, a key enzyme for the internalization of SARS-CoV-2 into the cells. The [Cu(Citr)(Bipy)] complex ranks just below the ones with Arg, Orn, and Lys complexes and is better than Nafamostat, Casiopeinas Cas III-ia, and Cas XI-Gly. As the serine protease TMPRSS2 could be an excellent target to stop the virus from getting inside the cell, the analyzed complexes are an excellent place to start looking for new drugs to treat COVID-19. On the other hand, copper complexes may be better for treating cancer than Pt(II) complexes because they are less toxic, work differently, have a different range of activity, and may not cause cross-resistance [67].

5. Conclusions

A new water-soluble Citrulline-copper mixed complex was synthesized and characterized as part of our search for Casiopeina© analogs. As for the aminoacidato complexes, the amino group's nitrogen and the carboxyl group's oxygen are coordinated to the copper atom. The carbonyl group of the ureide moiety is not coordinated in the axial positions; instead, these positions are occupied by an H_2O molecule and a nitrate ion, making an elongated octahedron around the copper due to a Jahn–Teller effect. The mononuclear compounds interact with one another through intermolecular hydrogen bonds between the coordinated water molecule and the carboxylate group of another compound. In addition, each compound interacts with a third entity thanks to the water molecule of crystallization, which joins the carboxyl group of one entity and the ureide group of another.

In contrast to previous work on copper bis-citrullinato, the resulting compound has a high water-solubility and a non-polymeric structure, which may be advantageous as the biological activity can be better estimated as it is not dose-limited. The theoretical calculations based on the DFT methodology were used to compare and characterize the bands and peaks of the UV/Vis, IR, and Raman spectra. All of them were in agreement with the experimental measurements. Non-covalent interactions analysis utilizing atoms in molecules (AIM) and Hirshfeld surface (HS) analyses showed high interaction energies between Citrulline and 2,2′-Bipyridine coordinated to Cu(II) in equatorial positions. Contrary, in axial positions, the NO_3^- ion and H_2O molecule are coordinated weakly, contributing to the distorted octahedral geometry of the complex.

This ternary complex containing Citrulline and 2,2′-Bipyridine will be used for preliminary biological studies using calf thymus DNA (CT-DNA) and plasmid pUC19 as a first approximation to cytotoxic activity against cancer cell lines.

Supplementary Materials: The following supporting information can be downloaded at https://www.mdpi.com/article/10.3390/cryst13091391/s1: Figure S1. ORTEP diagram of D, L pairs of the $[Cu(C_6H_{12}N_3O_3)(C_{10}H_{10}N_2)(NO_3)H_2O]$ complex. Ellipsoids are drawn at the 50% probability level; Figure S2. Enantiomers L, L, D, D, and D, L; Table S1: Crystal Data; Table S2: Fractional atomic coordinates and isotropic or equivalent isotropic displacement parameters (Å^2) for (a61322_mo), Table S3: Atomic displacement parameters (Å^2) for (a61322_mo).

Author Contributions: Conceptualization, D.R.-C. and E.G.-V.; Data curation, D.R.-C., Á.M. and M.E.C.; Investigation, A.G.-G., F.J.M. and E.G.-V.; Methodology, D.R.-C., A.G.-G., Á.M., L.E.S.-d.l.R., F.J.M., M.E.C. and E.G.-V.; Software, F.J.M. and M.E.C.; Writing—original draft, M.E.C. and E.G.-V.; Writing—review and editing, B.L.S.-G. All authors have read and agreed to the published version of the manuscript.

Funding: Project 100517029-VIEP (BUAP, México), the PRODEP Academic Group BUAP-CA-263 (SEP, Mexico), and the Ministerio de Universidades and Next Generation for the Margarita Salas contract 401 (Spain) funded this research.

Data Availability Statement: Data can be obtained directly from the authors upon request.

Acknowledgments: Diego Ramírez-Contreras wishes to thank CONAHCYT (Mexico) M.Sc. fellowship support number 1143792. María Eugenia Castro and Francisco J. Melendez wishes to thank Laboratorio Nacional de Supercómputo del Sureste de México (LNS-BUAP) and the CONAHCYT network of national laboratories for the computer resources and support provided. Amalia García-García thanks the Ministerio de Universidades and funds Next Generation (Spain).

Conflicts of Interest: The authors declare no conflict of interest.

References

1. Aguayo, E.; Martínez-Sánchez, A.; Fernández-Lobato, B.; Alacid, F. L-Citrulline: A Non-Essential Amino Acid with Important Roles in Human Health. *Appl. Sci.* **2021**, *11*, 3293. [CrossRef]
2. Zamuz, S.; Munekata, P.E.S.; Gullón, B.; Rocchetti, G.; Montesano, D.; Lorenzo, J.M. *Citrullus lanatus* as source of bioactive components: An up-to-date review. *Trends Food Sci. Technol.* **2021**, *111*, 208–222. [CrossRef]
3. Wada, M. On the Occurrence of a New Amino Acid in Watermelon, Citrullus Vulgaris, Schrad. *Bull. Agric. Chem. Soc. Japan* **1930**, *6*, 32–34. [CrossRef]
4. Fragkos, K.C.; Forbes, A. Was Citrulline First a Laxative Substance? The Truth about Modern Citrulline and Its Isolation. *Nihon Ishigaku Zasshi* **2011**, *57*, 275–292.
5. Manivannan, A.; Lee, E.-S.; Han, K.; Lee, H.-E.; Kim, D.-S. Versatile nutraceutical potentials of watermelon—A modest fruit loaded with pharmaceutically valuable phytochemicals. *Molecules* **2020**, *25*, 5258. [CrossRef]
6. Rimando, A.M.; Perkins-Veazie, P.M. Determination of citrulline in watermelon rind. *J. Chromatogr. A* **2005**, *1078*, 196–200. [CrossRef]
7. Curis, E.; Crenn, P.; Cynober, L. Citrulline and the gut. *Curr. Opin. Clin. Nutr. Metab. Care* **2007**, *10*, 620–626. [CrossRef]
8. Papadia, C.; Osowska, S.; Cynober, L.; Forbes, A. Citrulline in Health and Disease. Review on Human Studies. *Clin. Nutr.* **2018**, *37*, 1823–1828. [CrossRef] [PubMed]
9. Curis, E.; Nicolis, I.; Moinard, C.; Osowska, S.; Zerrouk, N.; Bénazeth, S.; Cynober, L. Almost all about Citrulline in mammals. *Amino Acids* **2005**, *29*, 177–205. [CrossRef]
10. Kurtz, A.C. A Simple Synthesis of *dl*-Citrulline. *J. Biol. Chem.* **1938**, *122*, 477–484. [CrossRef]
11. Ganadu, M.L.; Leoni, V.; Crisponi, G.; Nurchi, V. An investigation on the interaction between palladium(II) and L-citrulline by ^{1}H and ^{13}C NMR spectroscopy and potentiometry. *Polyhedron* **1991**, *10*, 333–336. [CrossRef]
12. Mascaliovas, B.Z.; Bergamini, F.R.G.; Cuin, A.; Corbi, P.P. Synthesis and crystal structure of a palladium(II) complex with the amino acid L-citrulline. *Powder Diffr.* **2015**, *30*, 357–361. [CrossRef]
13. Ramírez-Contreras, D.; García-García, A.; Sánchez-Gaytán, B.L.; Serrano-de la Rosa, L.E.; Melendez, F.J.; Choquesillo-Lazarte, D.; Rodríguez-Diéguez, A.; Castro, M.E.; González-Vergara, E. Bis-Citrullinato Copper(II) Complex: Synthesis, Crystal Structure, and Non-Covalent Interactions. *Crystals* **2022**, *12*, 1386. [CrossRef]
14. González-Ballesteros, M.M.; Mejía, C.; Ruiz-Azuara, L. Metallodrugs: An approach against invasion and metastasis in cancer treatment. *FEBS Open Bio* **2022**, *12*, 880–899. [CrossRef] [PubMed]
15. Molinaro, C.; Martoriati, A.; Pelinski, L.; Cailliau, K. Copper Complexes as Anticancer Agents Targeting Topoisomerases I and II. *Cancers* **2020**, *12*, 2883. [CrossRef]
16. Chavez-Gonzalez, A.; Centeno-Llanos, S.; Moreno-Lorenzana, D.; Sandoval-Esquivel, M.A.; Aviles-Vazquez, S.; Bravo-Gomez, M.E.; Ruiz-Azuara, L.; Ayala-Sanchez, M.; Torres-Martinez, H.; Mayani, H. Casiopeina III-Ea, a copper-containing small molecule, inhibits the in vitro growth of primitive hematopoietic cells from chronic myeloid leukemia. *Leuk. Res.* **2017**, *52*, 8–19. [CrossRef]
17. Bravo-Gómez, M.E.; García-Ramos, J.C.; Gracia-Mora, I.; Ruiz-Azuara, L. Antiproliferative activity and QSAR study of copper(II) mixed chelate [Cu(N-N)(acetylacetonato)]NO_3 and [Cu(N-N)(glycinato)]NO_3 complexes, (Casiopeínas). *J. Inorg. Biochem.* **2009**, *103*, 299–309. [CrossRef]
18. Trejo-Solís, C.; Palencia, G.; Zúñiga, S.; Rodríguez-Ropon, A.; Osorio-Rico, L.; Luvia, S.T.; Gracia-Mora, I.; Marquez-Rosado, L.; Sánchez, A.; Moreno-García, M.E.; et al. Cas IIgly induces apoptosis in glioma C6 cells in vitro and in vivo through caspase-dependent and caspase-independent mechanisms. *Neoplasia* **2005**, *7*, 563–574. [CrossRef]
19. Kachadourian, R.; Brechbuhl, H.M.; Ruiz-Azuara, L.; Gracia-Mora, I.; Day, B.J. Casiopeína IIgly-induced oxidative stress and mitochondrial dysfunction in human lung cancer A549 and H157 cells. *Toxicology* **2010**, *268*, 176–183. [CrossRef]

20. Martínez-Valencia, B.; Corona-Motolinia, N.D.; Sánchez-Lara, E.; Noriega, L.; Sánchez-Gaytán, B.L.; Castro, M.E.; Meléndez-Bustamante, F.; González-Vergara, E. Cyclo-tetravanadate bridged copper complexes as potential double bullet pro-metallodrugs for cancer treatment. *J. Inorg. Biochem.* **2020**, *208*, 111081. [CrossRef]
21. Martínez-Valencia, B.; Corona-Motolinia, N.D.; Sánchez-Lara, E.; Sánchez-Gaytán, B.L.; Cerro-López, M.; Mendoza, A.; Castro, M.E.; Meléndez-Bustamante, F.J.; González-Vergara, E. Synthesis and Experimental-Computational Characterization of a Copper/Vanadium Compound with Potential Anticancer Activity. *Crystals* **2020**, *10*, 492. [CrossRef]
22. Corona-Motolinia, N.D.; Martínez-Valencia, B.; Noriega, L.; Sánchez-Gaytán, B.L.; Mendoza, A.; Meléndez-Bustamante, F.J.; Castro, M.E.; González-Vergara, E. Ternary Copper Complex of L-Glutamine and Phenanthroline as Counterions of Cyclo-Tetravanadate Anion: Experimental–Theoretical Characterization and Potential Antineoplastic Activity. *Metals* **2021**, *11*, 1541. [CrossRef]
23. Vazquez-Rodriguez, S.; Ramírez-Contreras, D.; Noriega, L.; García-García, A.; Sánchez-Gaytán, B.L.; Melendez, F.J.; Castro, M.E.; González-Vergara, E. Interaction of copper potential metallodrugs with TMPRSS2: A comparative study of docking tools and its implications on COVID-19. *Front. Chem.* **2023**, *11*, 1128859. [CrossRef]
24. Su, C.-C.; Tai, T.-Y.; Wu, S.-P.; Wang, S.-L.; Liao, F.-L. Spectroscopic and electronic properties of mixed ligand aminoacidatocopper(II) complexes: Molecular structure of [Cu(4,7-dimethyl-1,10-phenanthroline)(L-phenylalaninato)](ClO_4). *Polyhedron* **1999**, *18*, 2361–2368. [CrossRef]
25. *CrysAlisCCD, CrysAlisRED*; Version 1.171.35.11; Oxford_Diffraction: Yarnton, UK, 2009.
26. Sheldrick, G.M. SHELXT—Integrated Space-Group and Crystal-Structure Determination. *Acta Crystallogr. Sect. A Found. Adv.* **2015**, *71*, 3–8. [CrossRef]
27. Dolomanov, O.V.; Bourhis, L.J.; Gildea, R.J.; Howard, J.A.K.; Puschmann, H. OLEX2: A complete structure solution, refinement and analysis program. *J. Appl. Crystallogr.* **2009**, *42*, 339–341. [CrossRef]
28. Hohenberg, P.; Kohn, W. Inhomogeneous Electron Gas. *Phys. Rev.* **1964**, *136*, B864–B871. [CrossRef]
29. Adamo, C.; Jacquemin, D. The calculations of excited-state properties with Time-Dependent Density Functional Theory. *Chem. Soc. Rev.* **2013**, *42*, 845–856. [CrossRef]
30. Adamo, C.; Barone, V. Toward reliable density functional methods without adjustable parameters: The PBE0 model. *J. Chem. Phys.* **1999**, *110*, 6158–6169. [CrossRef]
31. Hay, P.J.; Wadt, W.R. Ab initio effective core potentials for molecular calculations. Potentials for K to Au including the outermost core orbitals. *J. Chem. Phys.* **1985**, *82*, 299–310. [CrossRef]
32. Marenich, A.V.; Cramer, C.J.; Truhlar, D.G. Universal Solvation Model Based on Solute Electron Density and on a Continuum Model of the Solvent Defined by the Bulk Dielectric Constant and Atomic Surface Tensions. *J. Phys. Chem. B* **2009**, *113*, 6378–6396. [CrossRef] [PubMed]
33. Jin, Y.X.; Zhong, A.G.; Zhang, Y.J.; Pan, F.Y. Synthesis, crystal structure, spectroscopic properties, antibacterial activity and theoretical studies of a novel difunctional acylhydrazone. *J. Mol. Struct.* **2011**, *1002*, 45–50. [CrossRef]
34. Frisch, M.J.; Trucks, G.W.; Schlegel, H.B.; Scuseria, G.E.; Robb, M.A.; Cheeseman, J.R. *Gaussian 16*; Revision, B.01; Gaussian Inc.: Wallingford, CT, USA, 2016.
35. Dennington, R.D.; Keith, T.A.; Millam, J.M. *GaussView*; Version 6.0.16; Semi-Chem Inc.: Shawnee Mission, UK, 2016.
36. Keith, T.A. *TK Gristmill Software*; Version 19.02.13; AIMAll: Overland Park, KS, USA, 2019.
37. Turner, M.J.; MacKiinnon, J.J.; Wolff, S.K.; Grimwood, D.J.; Spackman, P.R.; Jayatilaka, D.; Spackman, M.A. CrystalExplorer17. Available online: https://crystalexplorer.scb.uwa.edu.au/ (accessed on 24 July 2023).
38. Halcrow, M.A. Jahn-Teller distortions in transition metal compounds, and their importance in functional molecular and inorganic materials. *Chem. Soc. Rev.* **2013**, *42*, 1784–1795. [CrossRef] [PubMed]
39. Veidis, M.V.; Schreiber, G.H.; Gough, T.E.; Palenik, G.J. Jahn-Teller distortions in octahedral copper (II) complexes. *J. Am. Chem. Soc.* **1969**, *91*, 1859–1860. [CrossRef]
40. Smith, D.W. Ligand field splittings in copper(II) compounds. In *Structure and Bonding*; Cardin, C., Duan, X., Gade, L.H., Sainz, L.G.-H., Lu, Y., Macgregor, S.A., Pariente, J.P., Schneider, S., Stalke, D., Eds.; Springer: Berlin/Heidelberg, Germany, 1972; Volume 12, pp. 49–112.
41. Hathaway, B.J. A new look at the stereochemistry and electronic properties of complexes of the copper(II) ion. In *Complex Chemistry. Structure and Bonding*; Emslev, J., Ernst, R.D., Hathaway, B.J., Warren, K.D., Eds.; Springer: Berlin/Heidelberg, Germany, 1984; Volume 57, pp. 55–118.
42. Stanila, A.; Marcu, A.; Rusu, D.; Rusu, M.; David, L. Spectroscopic studies of some copper(II) complexes with amino acids. *J. Mol. Struct.* **2007**, *834–836*, 364–368. [CrossRef]
43. Cuevas, A.; Viera, I.; Torre, M.H.; Kremer, E.; Etcheverry, S.B.; Baran, E.J. Infrared Spectra of the Copper(II) Complexes of Amino Acids with Hydrophobic Residues. *Acta Farm. Bonaer.* **1998**, *17*, 213–218.
44. Castellucci, E.; Angeloni, L.; Neto, N.; Sbrana, G. IR and Raman spectra of A 2, 2′-bipyridine single crystal: Internal modes. *Chem. Phys.* **1979**, *43*, 365–373. [CrossRef]
45. Jinnah, M.M.A.; Sasirekha, V.; Ramakrishnan, V. Vibrational spectral studies of l-citrullinium perchlorate. *Spectrochim. Acta A. Mol. Biomol. Spectrosc.* **2005**, *62*, 840–844. [CrossRef]
46. Baran, E.; Wagner, C.C.; Torre, M.; Kremer, E.; Kögerler, P. Vibrational spectra of the Cu(II) complexes of aspartic and glutamic acids. *Acta Farm. Bonaer.* **2000**, *19*, 231–234.

47. Zapata, F.; García-Ruiz, C. The discrimination of 72 nitrate, chlorate, and perchlorate salts using IR and Raman spectroscopy. *Spectrochim. Acta A. Mol. Biomol. Spectrosc.* **2018**, *189*, 535–542. [CrossRef]
48. Sreevalsa, V.G.; Jayalekshmi, S. Investigations on the Growth and Characterization of L-Citrulline Oxalate Monohydrate Single Crystal. *J. Cryst. Growth* **2011**, *324*, 172–176. [CrossRef]
49. Strukl, J.S.; Walter, J.L. Infrared and Raman spectra of heterocyclic compounds—III: The infrared studies and normal vibrations of 2,2′-bipyridine. *Spectrochim. Acta A. Mol. Spectrosc.* **1971**, *27*, 209–221. [CrossRef]
50. Corona-Motolinia, N.D.; Martínez-Valencia, B.; Noriega, L.; Sánchez-Gaytán, B.L.; Méndez-Rojas, M.Á.; Melendez, F.J.; Castro, M.E.; González-Vergara, E. Synthesis, Crystal Structure, and Computational Methods of Vanadium and Copper Compounds as Potential Drugs for Cancer Treatment. *Molecules* **2020**, *25*, 4679. [CrossRef] [PubMed]
51. Caruso, A.; Rossi, M.; Gahn, C.; Caruso, F. A structural and computational study of Citrulline in biochemical reactions. *Struct. Chem.* **2017**, *28*, 1581–1589. [CrossRef]
52. Fu, R.; So, S.M.; Lough, A.J.; Chin, J. Hydrogen Bond Assisted L to D Conversion of Amino Acids. *Angew. Chem. Int. Ed.* **2020**, *59*, 4335–4339. [CrossRef] [PubMed]
53. Kolarovĭc, A.; Jakubec, P. State of the Art in Crystallization-Induced Diastereomer Transformations. *Adv. Synth. Catal.* **2021**, *363*, 4110–4158. [CrossRef]
54. Wang, Q.; Wang, Y.; Tang, J.; Yang, Z.; Zhang, L.; Huang, X. New insights into the interactions between Pb (II) and fruit waste biosorbent. *Chemosphere* **2022**, *303*, 135048. [CrossRef]
55. Singh, M.; Sinha, S.; Krishna, V. Computed Distribution of Quaternary Complexes of Cu (II), Zn (II) Co (II) and Ni (II) with Citrulline and Tryphtophan as Primary Ligand and Thymine as Secondary Ligand. *Proc. Natl. Acad. Sci. India Sect. A Phys. Sci.* **2021**, *91*, 1–7. [CrossRef]
56. Figueroa-DePaz, Y.; Resendiz-Acevedo, K.; Dávila-Manzanilla, S.G.; García-Ramos, J.C.; Ortiz-Frade, L.; Serment-Guerrero, J.; Ruiz-Azuara, L. DNA, a target of mixed chelate copper (II) compounds (Casiopeinas®) studied by electrophoresis, UV–vis and circular dichroism techniques. *J. Inorg. Biochem.* **2022**, *231*, 111772. [CrossRef]
57. Gracia-Mora, I.; Ruiz-Ramírez, L.; Gómez-Ruiz, C.; Tinoco-Méndez, M.; Márquez-Quiñones, A.; De Lira, L.R.; Marín-Hernández, A.; Macías-Rosales, L.; Bravo-Gómez, M.E. Knigth's move in the periodic table, from copper to platinum, novel antitumor mixed chelate copper compounds, casiopeinas, evaluated by an in vitro human and murine cancer cell line panel. *Met.-Based Drugs* **2001**, *8*, 19–28. [CrossRef]
58. Santini, C.; Pellei, M.; Gandin, V.; Porchia, M.; Tisato, F.; Marzano, C. Advances in copper complexes as anticancer agents. *Chem. Rev.* **2014**, *114*, 815–862. [CrossRef] [PubMed]
59. Carvallo-Chaigneau, F.; Trejo-Solís, C.; Gómez-Ruiz, C.; Rodríguez-Aguilera, E.; Macías-Rosales, L.; Cortés-Barberena, E.; Cedillo-Peláez, C.; Gracia-Mora, I.; Ruiz-Azuara, L.; Madrid-Marina, V.; et al. Casiopeina III-ia induces apoptosis in HCT-15 cells in vitro through caspase-dependent mechanisms and has antitumor effect in vivo. *BioMetals* **2008**, *21*, 17–28. [CrossRef] [PubMed]
60. Gutiérrez, A.G.; Vázquez-Aguirre, A.; García-Ramos, J.C.; Flores-Alamo, M.; Hernández-Lemus, E.; Ruiz-Azuara, L.; Mejía, C. Copper(II) mixed chelate compounds induce apoptosis through reactive oxygen species in neuroblastoma cell line CHP-212. *J. Inorg. Biochem.* **2013**, *126*, 17–25. [CrossRef] [PubMed]
61. Hernández-Esquivel, L.; Marín-Hernández, A.; Pavón, N.; Carvajal, K.; Moreno-Sánchez, R. Cardiotoxicity of copper-based antineoplastic drugs casiopeinas is related to inhibition of energy metabolism. *Toxicol. Appl. Pharmacol.* **2006**, *212*, 79–88. [CrossRef]
62. Marín-Hernández, A.; Gracia-Mora, I.; Ruiz-Ramírez, L.; Moreno-Sánchez, R. Toxic effects of copper-based antineoplastic drugs (Casiopeinas®) on mitochondrial functions. *Biochem. Pharmacol.* **2003**, *65*, 1979–1989. [CrossRef] [PubMed]
63. Serment-Guerrero, J.; Bravo-Gomez, M.E.; Lara-Rivera, E.; Ruiz-Azuara, L. Genotoxic assessment of the copper chelated compounds Casiopeinas: Clues about their mechanisms of action. *J. Inorg. Biochem.* **2017**, *166*, 68–75. [CrossRef]
64. Becco, L.; García-Ramos, J.C.; Ruiz-Azuara, L.; Gambino, D.; Garat, B. Analysis of the DNA interaction of copper compounds belonging to the Casiopeinas Antitumoral series. *Biol. Trace Elem. Res.* **2014**, *161*, 210–215. [CrossRef]
65. Bravo-Gómez, M.E.; Campero-Peredo, C.; García-Conde, D.; Mosqueira-Santillán, M.J.; Serment-Guerrero, J.; Ruiz-Azuara, L. DNA-binding mode of antitumoral copper compounds (Casiopeinas®) and analysis of its biological meaning. *Polyhedron* **2015**, *102*, 530–538. [CrossRef]
66. Reina, M.; Talavera-Contreras, L.G.; Figueroa-DePaz, Y.; Ruiz-Azuara, L.; Hernández-Ayala, L.F. Casiopeinas® as SARS-CoV-2 main protease (Mpro) inhibitors: A combined DFT, molecular docking and ONIOM approach. *New J. Chem.* **2022**, *46*, 12500–12511. [CrossRef]
67. Lucaciu, R.L.; Hangan, A.C.; Sevastre, B.; Oprean, L.S. Metallo-drugs in cancer therapy: Past, present and future. *Molecules* **2022**, *27*, 6485. [CrossRef]